Electronic Supplementary Material (ESI) for Journal of Materials Chemistry C.

Supplementary information

Critical Transition to a Highly Conductive State through PEDOT Oligomer Percolation in Redox-Active COFs

Section 1. Materials and instrumentation

1.1 Materials

2,4,6-triformylphloroglucinol (TIC), 2,6-diaminoanthraquinone (TIC), 2, 5-dibromo-3, 4-ethylenediooxythiophene (TIC), sodium hydrosulfite (wako), Dimethylacetamide (wako), mesitylene (wako), N-Methyl-2-Pyrrolidone (wako).

1.2 Instrumentation

Powder x-ray diffraction (PXRD). The PXRD data were collected on a PANalytical X Pert Pro diffractometer with Cu Kα radiation of λ=1.5418 Å at 40 kV and 40 mA.

Nitrogen (N_2) gas adsorption. Adsorption-desorption experiments were conducted on a BELSORP-min surface arear and porosimeters analyzer. The sample was degassed at 120℃ for 24 h before the measurement. N_2 isotherms were recorded at 77 K by using ultra-high purity N_2 (99.999％ purity). Data analyses were conducted using BEL master TM software. The surface area was determined using Brunauer-Emmett-TELLER (BET) adsorption model, and the pore volume was determined using the single point adsorption model and provided in the main text. The pore size distribution was calculated from the adsorption isotherm by nonlocal density functional theory (NLDF) method and provided in the main text.

Others. Fourier transform infrared (FT-IR). Spectra were recorded on a Perkin Elmer spectrum one FT-IR spectrometer using ATR. Scanning electron microscope (SEM) image were obtained on a Hitachi S-4300 with an acceleration volage of 5 kV and emission current of 10 μA. Electron paramagnetic resonance (EPR) spectrum were collected with a JEOL JES-FA200, the central field was set 300mT and the range of scan was 100mT. Electrochemical experiments were conducted on a biologic SP-150 single potentiostat electrochemical analyzer using a standard three-electrode system in 1M H_2SO_4 aqueous solution. Glassy carbon (GC) electrodes were coated with the active materials. Pt wire was used as the working electrode, while an aqueous Ag/AgCl electrode served as the reference electrode.

Section 2. Synthesis of AQ-COF, PEDOT@AQ-COF and PEDOT

2.1. AQ-COF

A 10 ml Pyrex tube was charged with 2,4,6-triformylphloroglucinol (TFP, 40 mg, 0.2 mmol), 2,6-diaminoanthraquinone (DAAQ, 68 mg, 0.3 mmol), Dimethylacetamide/mesitylene (2.4 ml, 3/1 by vol), then 0.1 ml of aqueous acetic acid (6 M) was added. The resulting mixture was sonicated for 1 minute at room temperature and degassed via 2 freeze-pump-thaw cycles. The tube was sealed under vacuum heated at 120 for 3 days. The reaction mixture was cooled to room temperature and the dark-red precipitate was collected by centrifugation and washed with DMF and acetone. The powder was exhaustively washed Soxhlet extractions with THF for 24 hours and then dried under vacuum at 120％ overnight to afford a red powder. Yield：80％.

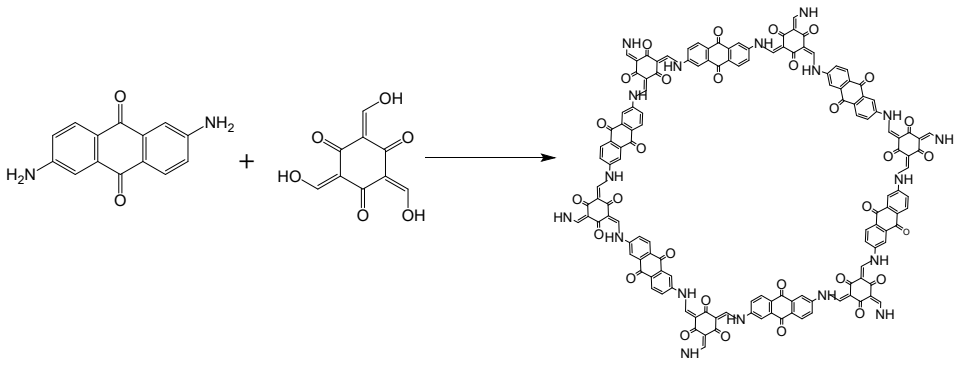

2.2. PEDOT@AQ-COF (Samples 1 to 7)

A 30 ml glass vial was charged with 2, 5-dibromo-3, 4-ethylenediooxythiophene(DBrEDOT, 270 mg), acetone (11 mL), then AQ-COF (200 mg) was add to the solution and stirred at 25℃ for 2 hour. The acetone was then evaporated under reduced pressure (20 kPa, 25℃). The obtained red powder was washed with hexane (5 mL) to remove the surface DBrDOT, dried under vacuum and sealed into glass vial under nitrogen. Then the glass vial was heated in an oven at 60℃ for 3 days and 85℃ for a day. The DBrDOT polymerized in the channel of the AQ-COF, giving a solid-state black composite of PEDOT@AQ-COF. After cooling down, the black powder was washed with 10 mL of acetone, 20 ml of aqueous sodium hydrosulfite (1M), 20 ml of water and 10 mL of acetone. The powder was dried under vacuum at 120℃ overnight, give Sample **1**.[1]

The other samples were synthesized by the same mothed. The DBrDOT was set in different amount (which was 300 mg, 330 mg, 360 mg, 390 mg, 420 mg, 450 mg), then was dissolved in acetone (12 ml, 13ml, 14 ml, 15 ml, 16 ml, 17 ml), and the solution was add 200 mg of AQ-COF. After the reaction, we obtained samples **2** to **7**, respectively. Elemental analysis of the calculated sample **1** $(C_{60}H_{30}N_6O_{12})\cdot(C_6H_4O_2S)_4\cdot(H_2O)_{5.5}\cdot Br$, C (54.63), H (3.12), N (4.55), S (6.94); found C (50.65), H (3.12), N (4.04), S (6.09), Br (7.65). Sample **2** $(C_{60}H_{30}N_6O_{12})\cdot(C_6H_4O_2S)_6\cdot(H_2O)_{8.5}\cdot Br_{1.2}$, C (52.87), H (3.34), N (3.85), S (8.81); found C (49.30), H (3.34), N (3.42), S (8.06), Br(8.95). Sample **3** $(C_{60}H_{30}N_6O_{12})\cdot(C_6H_4O_2S)_{6.7}\cdot(H_2O)_{10.7}\cdot Br_{1.2}$, C (51.88), H (3.40), N (3.63), S (9.25) Br (); found C (48.94), H (3.40), N (3.53), S (8.99), Br (8.05). Sample **4** $(C_{60}H_{30}N_6O_{12})\cdot(C_6H_4O_2S)_{7.8}\cdot(H_2O)_{10}\cdot Br_{2.3}$, C (52.14), H (3.26), N (3.42), S (10.15); found C (44.86), H (3.26), N (2.85), S (8.84) Br (12.28). Sample **5** $(C_{60}H_{30}N_6O_{12})\cdot(C_6H_4O_2S)_{8.1}\cdot(H_2O)_{11.4}\cdot Br_{2.2}$, C (51.60), H (3.36), N (3.33), S (10.26); found C (44.32), H (3.36), N (2.97), S (9.02) Br (13.23). Sample **6** $(C_{60}H_{30}N_6O_{12})\cdot(C_6H_4O_2S)_{7.7}\cdot(H_2O)_{10.6}\cdot Br_{1.4}$, C (51.89), H (3.25), N (3.42), S (10.04); found C (48.08), H (3.25), N (3.11), S (9.05), Br (8.30). sample **7** $(C_{60}H_{30}N_6O_{12})\cdot(C_6H_4O_2S)_{8.3}\cdot(H_2O)_{11.0}\cdot Br_{1.7}$, C (51.69), H (3.35), N (3.30), S (10.42); found C (46.47), H (3.35), N (2.98), S (9.54), Br (10.01).

2.3. PEDOT

A glass vial was charged with 300 mg of 2,5-Dibromo-3,4-ethylenedioxythiophene (DBrDOT), and was sealed under nitrogen. Then the glass vial was heated in an oven at 60℃ for 3 days and 85℃ for a day. After cooling down, the black powder was washed with 10 mL of acetone, 20 mL of aqueous

sodium hydrosulfite (1 M), 20 mL of water and 10 mL of acetone. After that, the powder was dried under vacuum at 120℃ overnight. Giving a black powder PEDOT.

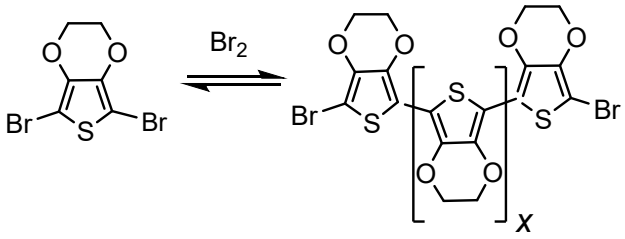

Section 3. CV, EIS and conductivity measurements

3.1. Electrode preparations

The PEDOT@AQ-COF (90 wt%) and polyvinylidene fluoride (PVDF) binder (10 wt%) were dispersed in of N-Methyl-2-Pyrrolidone (NMP) and obtained ink-like slurry. Which was coated on the top of a GC electrode. The diameter of the GC is 5 mm, and the loading of the active materials was measured to be 0.51mg/cm^2.

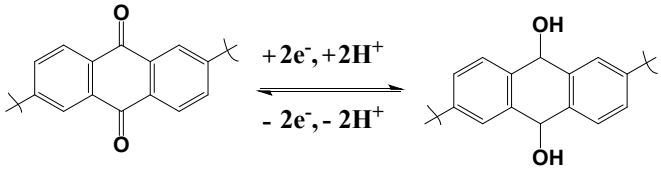

3.2. Two-probe measurements

50 mg of sample was added to a stander 10 mm die, then pressed under 100 KN for 1 hour and give a pellet. The pellet was cut into rectangle. The gold wire of dimeter 25 μm was attached to the pellet with gold paste. After drying, the pellet was connected to the probe. the sample was measured to investigated in the two-probe voltage-applying current measurement *(I-V)* method by an ADVANTEST R6245 source meter controlled by a PC through the GP-IB interface with custom-made software. The temperature dependence of the conductivity was measure upon cooling in the temperature range from 298 to 77 K.

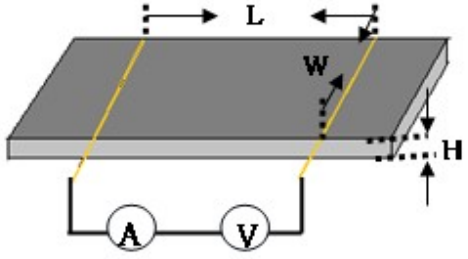

Section 4. Characterization

4.1. FT-IR

The AQ-COF shows the characteristic absorbances of β-ketoenamine linkage at 1235, 1555, and 1615 cm^{-1} are attributed to the C-N, C＝C, and C＝O bonds. The samples of DBrEDOT@AQ-COF show the weak characteristic C=C stretching peaks and inter-ring C-C stretching peaks around 1500-1300cm^{-1}, in addition, the peaks at 950, 865, 720 cm^{-1} are the absorbances of C-S-C stretching vibrations of thiophene ring. Comparing with the AQ-COF. The bending vibrations of the C-O bond of ethylenedioxy absorbances peaks also show in the samples at 1070 cm^{-1}. Indicated that the monomer DBrEDOT had been loaded into the channel of AQ-COF (Fig. S1). After polymerization, the samples of PEDOT@AQ-COF show characteristic absorbances of asymmetric C=C and inter-ring C-C stretching peaks around 1510 and 1315 cm^{-1}. Which indicated the formation of PEDOT (Fig. S2).

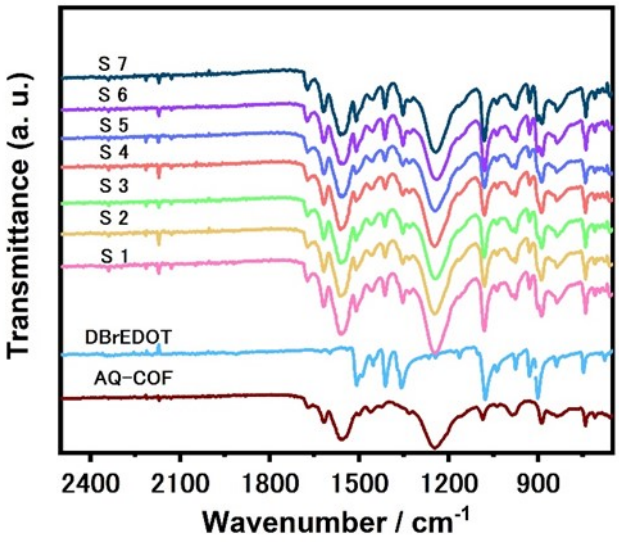

Figure S1. FT-IR spectra for AQ-COF, DBrDOT, and Samples **1** to **7** before polymerization.

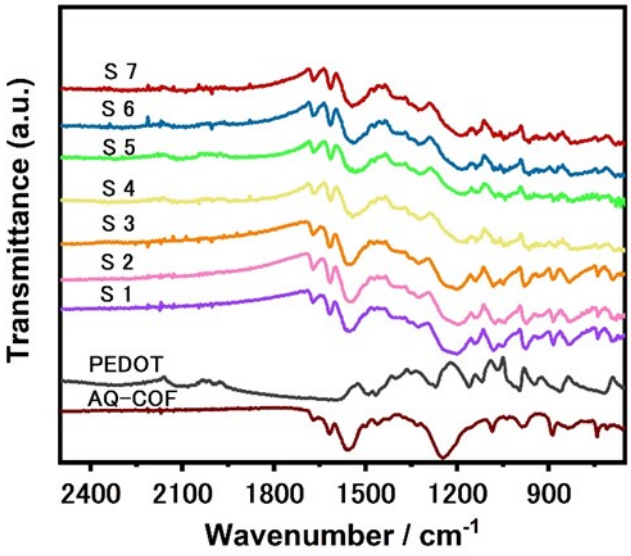

Figure S2. FT-IR spectra for AQ-COF, DBrDOT, and Samples **1** to **7** after polymerization.

4.2. PXRD

PXRD shows the AQ-COF with an intense diffraction peak at 3.5° (100), 7.0° (210), and a broad peak at 27°(001). Exhibit patterns of a 2D hexagonal network with a pore diameter of 2.3 nm. (Fig. S3) The peak at 3.5° (100) is not observed. After depositing the PEDOT within the ordered AQ-COF, which is indicated by the presence of guest PEDOT in the pores. A close broad peak at 26° was observed in the samples. That was explained by access bromine, which is kinetically trapped in the PEDOT lattice, is the most significant contributor to the amorphous part of the XRD spectra.

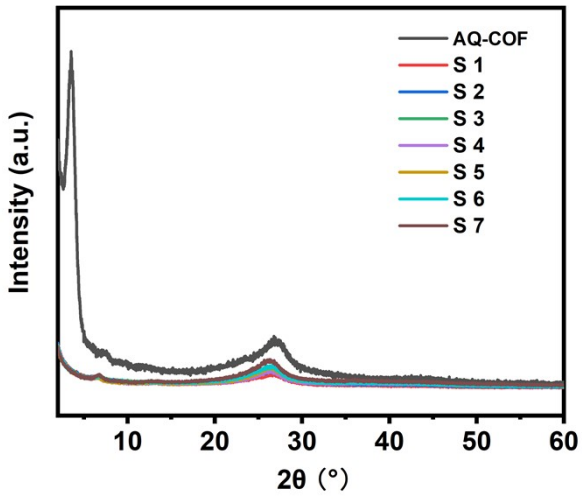

Figure S3. PXRD of AQ-COF and Samples **1** to **7**.

4.3. N_2 Sorption Isotherms

Figure S4 shows the N_2 sorption Isotherms of AQ-COF and Samples **1** to **7**. The AQ-COF exhibited a high surface area 851 m^2 g^{-1} compared with the other samples. The porosity of PEDOT@AQ-COF sharply decreased after PEDOT polymerization. As the concentration of PEDOT in the porose increased with a small gradient from Sample **1** to **7**, so porosity decreased in a narrow range.

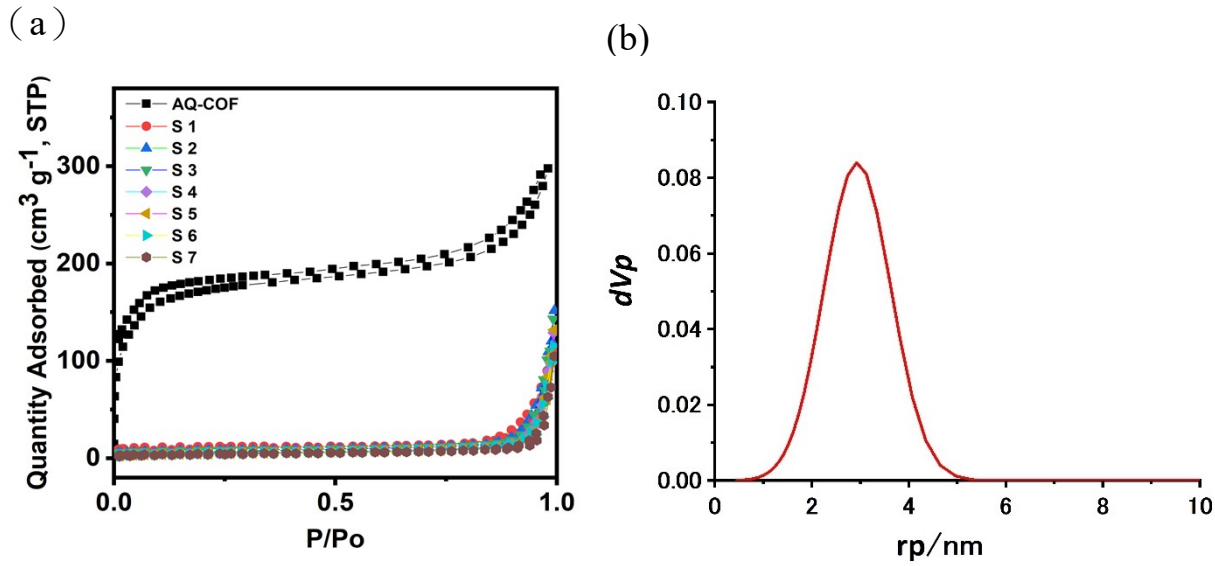

Figure S4. (a)N_2 sorption isotherms of AQ-COF and Samples **1** to **7**. (b) The AQ-COF Pore size distribution.

4.4. SEM

SEM images of samples **1** and **7** are shown in Figures S5(a) and (b), respectively, showing homogeneous particles. Panel (c) of this figure shows the results of a control experiment in which an excess amount of DBrEDOT was added to AQ-COF and PEDOT was grown outside of it. Figure S5(c) clearly shows needle-shaped PEDOT crystals. In other words, samples **1** and **7** do not contain freestanding PEDOT outside of AQ-COF because DBrEDOT outside of AQ-COF was removed by washing with acetone before polymerization.

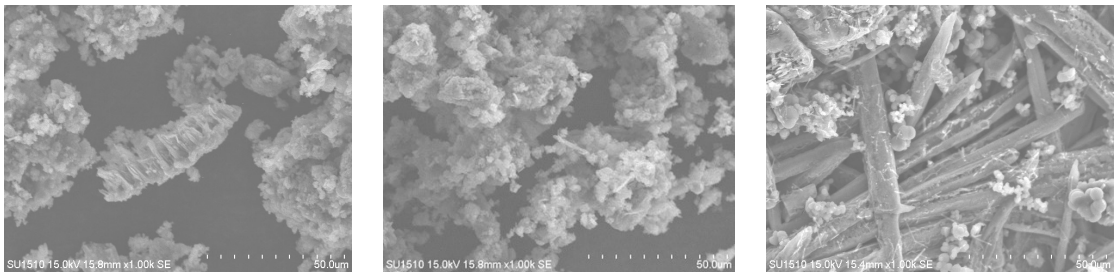

(a) (b) (c)

Figure S5. SEM of images for Sample **1** (a), Sample **7** (b) and the results of the control experiment.

Section 5. Electrical conductivity

Figure S6 shows the *I*-*V* plots for Samples **1** to **7** at room-temperature. The measurement methods are described in Section 3.2. Figure S7 shows the non-linear *I*-*V* curve of Sample **1**, measures at room temperature. It is considered that the applied high voltage would overcome a potential barrier for carriers between the hosts and/or between the host and guest, due to the unsaturation of conductive PEDOT chains in AQ-COF in Sample **1**

Figure S8 shows the temperature dependence of the conductivity of Samples **3** and **4**.

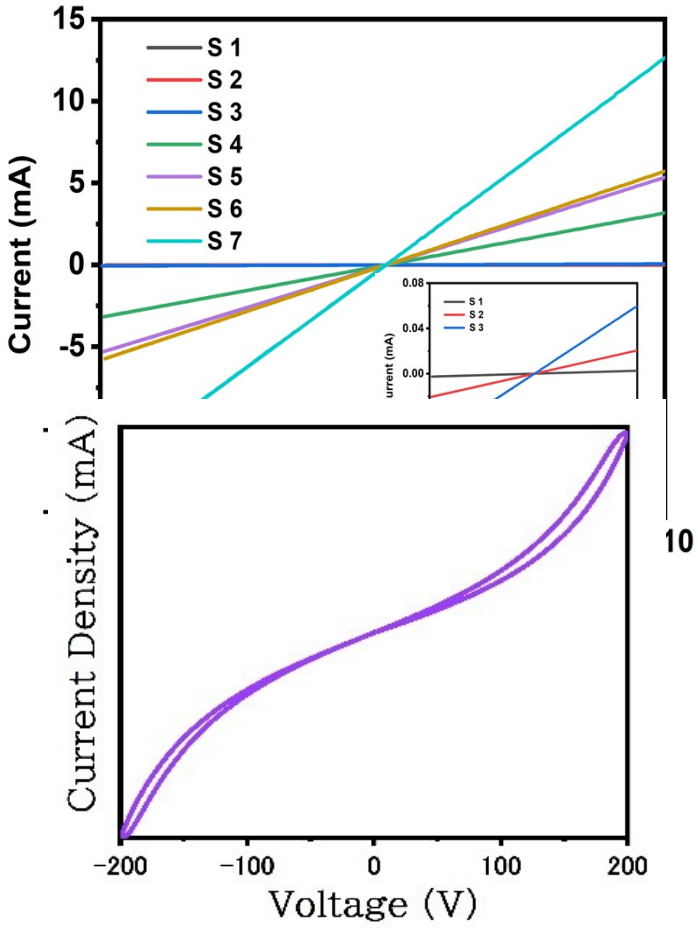

Figure S7. *I-V* plots for Sample **1** in the range between −200 and 200 V at room temperature.

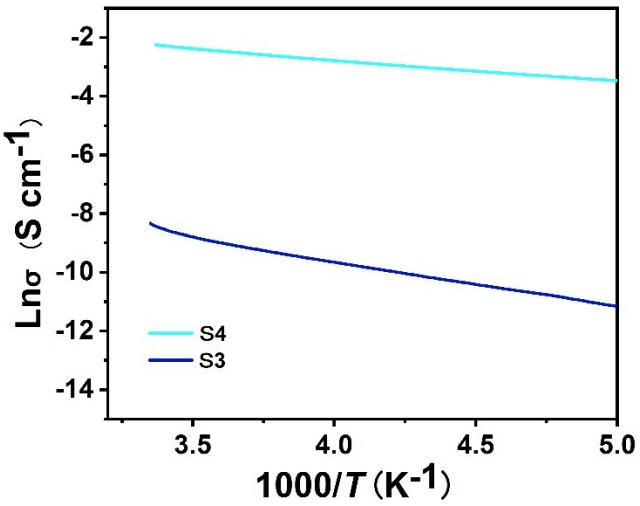

Figure S8. Arrhenius plots for the temperature dependence of the conductivities of Samples **3** and **4**.

Section 6. EPR

Figure S9 shows the EPR spectra of Samples **1** to **7** and Fig. S10 shows that of AQ-COF. They were measured at room temperature. Figures S11 ahd S12 show the temperaature dependence of the EPR spectra for Samples **4** and **1**, respectively. Figure S13 shows the temperature dependence of the g factors for Samples **1** and **4**.

Samples **1** and **4** exhibit the *g* factors -value of 2.004 (Fig. S13), indicating the possibility of homology radical in the samples. However, the radical is localized in Sample **1**, which fits Curie's law (Fig. 5a). On the other hand, Sample **4** fits χ_{EPR} =C/T + χ_0, where χ_0 is contributed by Pauli-like spin, which is delocalized charge carriers. Although Sample **1** and **4** have similar chain lengths (x=4.5 and 3.4, respectively), Sample **4** shows wider EPR linewidth which is characteristic degree of delocalization than the low conductive samples (Samples **1**~**3**) (see Fig. 4b). It is most likely that Sample **4** is doped with charge due to the reaction between the active group of AQ-COF and PEDOT, which promotes the delocalization and movement of electrons, improving conductivity sharply. However, the *g* factors of Samples **1** and **4** are nearly the same, as indicated in Fig. S13. This would be rationalized by the fact that the board peaks in the CV curves of the high conductive sample (Sample **4**~**7**) in Fig. 3(a) suggest a simultaneous 2-electron redox reaction of the quinone moiety that makes the radical species of AQ-COF unobservable.

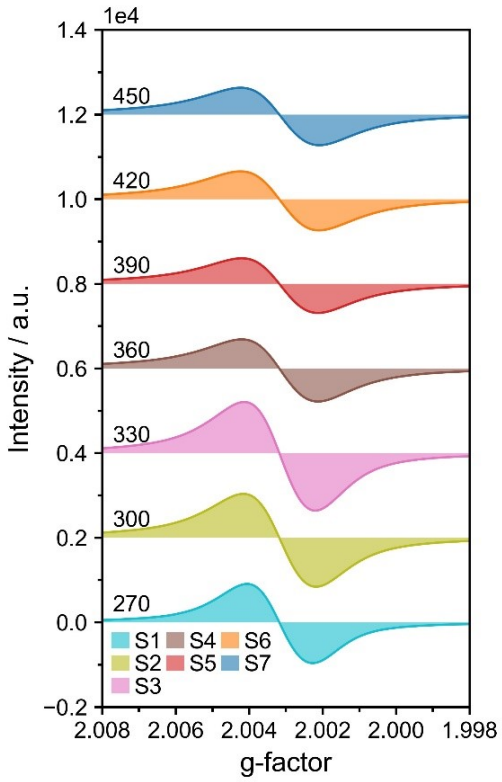

Figure S8. EPR spectra of Samples **1** to **7** at room temperature.

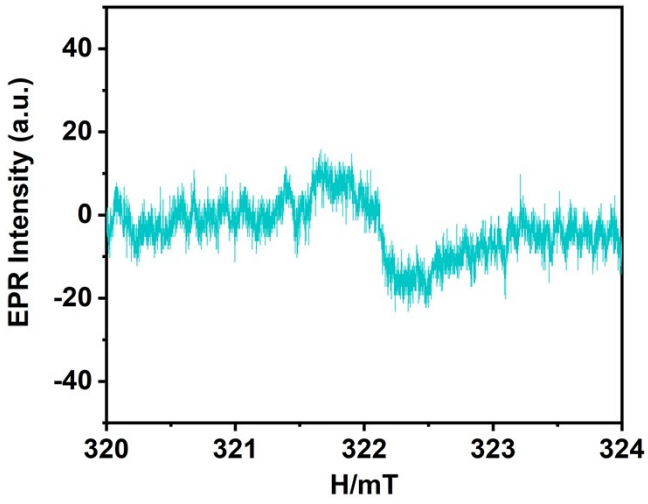

Figure S10. EPR spectrum of AQ-COF at room temperature.

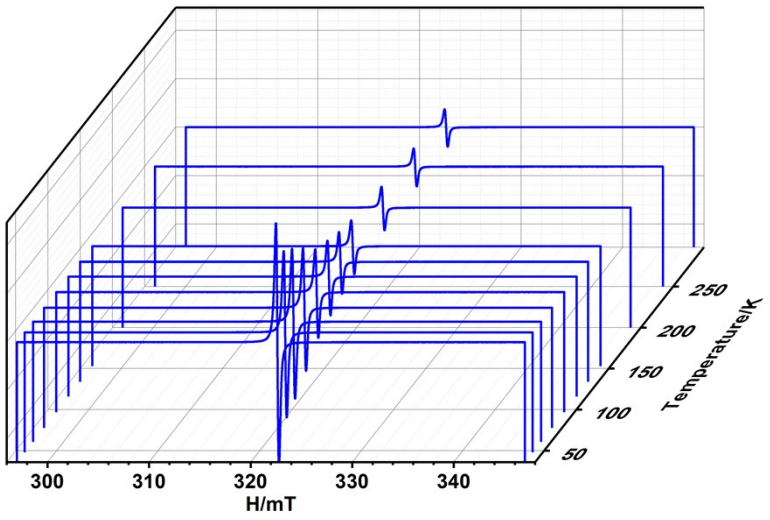

Figure S11. Temperature dependence of the EPR spectra for Sample **4**.

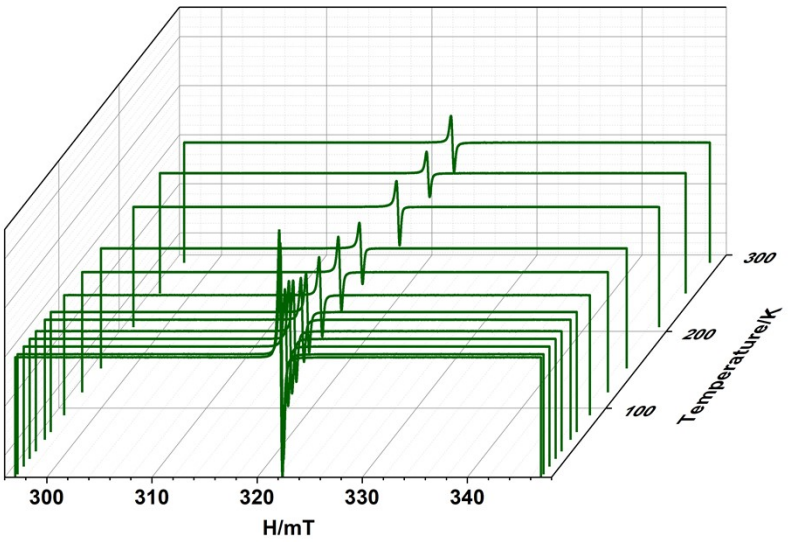

Figure S12. Temperature dependence of EPR spectra for sample **1**.

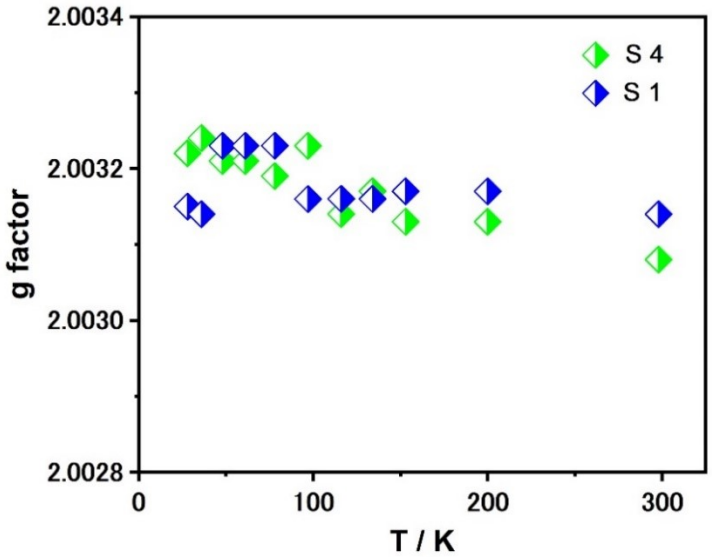

Figure S13. Temperature dependence of the *g* factors for Samples **1** and **4**.

Section 7. UV-vis-NIR

Kubelka–Munk function is definded as

$$F=(1-r)^2/2r$$

Solid-state UV-Vis-NIR spectra were measured for Samples **3** and **4**, and AQ-COF (Fig S14), which were prepared by the following procedure. 4 mg of sample and 200 mg of $BaSO_4$ were mixied and mechanical grinding to get uniform powder. Then the powder was coated on a sample holder. a JASCO V-570 spectrometer was used to record the UV-vis-NIR diffuse reflectance spectra. All samples were measure at room temperature. the mesured conditions: scan from 250 nm to 1900 nm with a bandwidth I nm, data acquisition interval of 0.1 nm, scanning speed of 100 nm/min.

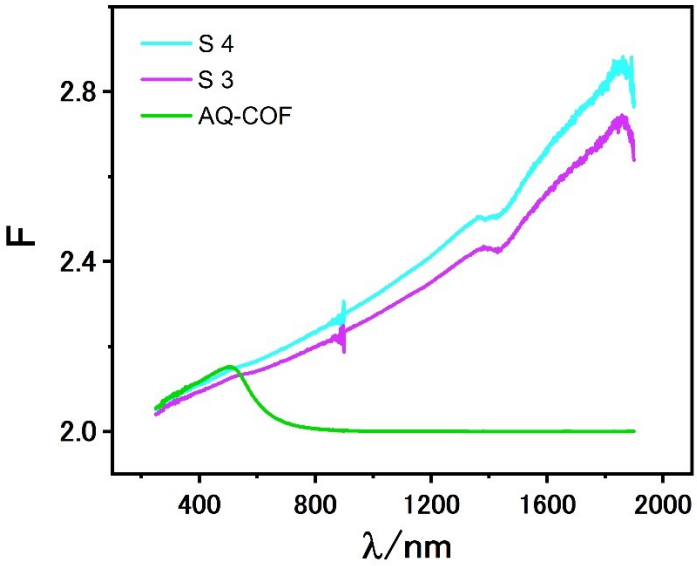

Figure S14. Wavelength λ dependence of Kubelka–Munk function *F* for Samples **3** and **4**, and AQ-COF.

Section 8. EIS Analysis

The mesearment is using the three-electrode configurations in 1 M H_2SO_4 electrolyte. The electrode prearation is shown in Section 3**.** The plots were obtaind by scanning fi 0.1 kHz to ff 100 mHz, with Nd 12, under the votage 5mT. Where fi is initial frequency, ff is final frequence, Nd is number of points per decade.

The sample **4** and **7** have the significant differentce from sample **2** and **3**. the sample **4** and **7** show the slash with higher slope than sample **2** and **3** indacated that, sample **4** and **7** behaver faster transfer rate of ion and higher electrochemical capacitance than sample **2** and **3**. Corresponding the CV curve (Fig.

3a) and high conductivity (Fig 2).

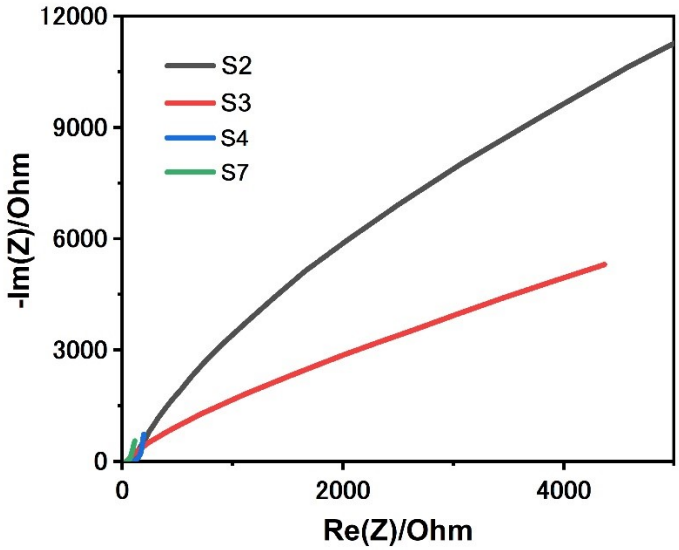

Figure S15. The EIS plot of Sample **2**, **3**, **4** and **7**.

Reference

1 Y. Wu, Z. Zhang, S. Bandow and K. Awaga, *Bull Chem Soc Jpn*, 2017, **90**, 1382–1387.

2 A. J. Kronemeijer, E. H. Huisman, I. Katsouras, P. A. van Hal, T. C. T. Geuns, P. W. M. Blom, S. J. van der Molen and D. M. de Leeuw, *Phys Rev Lett*, 2010, **105**, 156604.

3 K. Asadi, A. J. Kronemeijer, T. Cramer, L. Jan Anton Koster, P. W. M. Blom and D. M. de Leeuw, *Nat Commun*, 2013, **4**, 1710.

4 J. D. Yuen, R. Menon, N. E. Coates, E. B. Namdas, S. Cho, S. T. Hannahs, D. Moses and A. J. Heeger, *Nat Mater*, 2009, **8**, 572–575.

5 J. Wang, D. Liu, L. Yu, F. Liu, J. Niu, G. Yang, C. Lu, N. Lu, L. Li and M. Liu, *Phys Rev Lett*, 2023, **130**, 177001.

6 K. Mizoguchi, *Synth Met*, 2001, **119**, 35–38.

7 H. Eichele, M. Schwoerer, R. Huber and D. Bloor, *Chem Phys Lett*, 1976, **42**, 342–346.

8 R. Kiebooms, A. Aleshin, K. Hutchison, F. Wudl and A. Heeger, *Synth Met*, 1999, **101**, 436–437.